International Journal of Engineering Science Invention (IJESI)
ISSN (Online): 2319-6734, ISSN (Print): 2319-6726
www.ijesi.org ||Volume 9 Issue 8 Series I || August 2020 || PP 07-10

3-D exponentially Casson fluid-driven flow under inclined magnetic field: A convergent series expansion

EmranKhoshrouye Ghiasi[1], WuritiSridhar[2]
[1]*Young Researchers and Elite Club, Mashhad Branch, Islamic Azad University, Mashhad, Iran*
[2]*Department of Mathematics, KoneruLakshmaiah Education Foundation, Vaddeswaram, Guntur-522502, India*

ABSTRACT: *In this work, an additional convergence of the homotopic based approach is investigated for the three-dimensional (3-D) exponentially flow pattern subjected to inclined magnetic field. To this end, the auxiliary parameters contained in the series expansions are optimized by minimizing the square residual errors. After finding the CPU time incurred in each step, it is seen that the 9th-order homotopy based approach will converge with* $\hbar_{\varphi}$ *= -0.243 and* $\hbar_{\bar{\varphi}}$ *= -0.243 quickly.*

KEYWORDS -3D flow, Casson fluid, Magnetic field, Additional convergence, Relative error.

Date of Submission: 07-08-2020 Date of Acceptance: 21-08-2020

I. INTRODUCTION

Besides two-dimensional cases, 3-D examination of incompressible viscous fluids with different thermodynamic properties has been greatly developed over the last two decades. In general, analyzing the 3-D wall shear problems, which can be considered as the boundary-layer theory (BLT) [1], is very important nowadays. One of the most challenging questions associated with the BLT is to identify the flow separation which occurs in adverse pressure gradients [2]. In this way, Sandeep et al. [3] studied the 3-D unsteady Casson fluid-driven flow with thermal and solutal stratification phenomena, and found that the effect of thermal diffusion can be ignored only in the vicinity of the wall at absolute zero. Indeed, they could capture the velocity and temperature distributions for cases subjected to uniform heat energy and justify the two-step boundary layer development which had been discovered by Williams and Rhyne [4]. Another example is the use of homotopic based approach to analyze the chemical reaction dynamics arising in 3-D fluid-driven flow past a bidirectional wall which was represented by Shehzad et al. [5]. Furthermore, Nayak [6], Rehman et al. [7], Hayat et al. [8,9], Shehzad et al. [10,11], Alsaedi et al. [12], Ashraf et al. [13] and Lu et al. [14] provided some rigorous justification of the homotopic based approach to investigate the 3-D flow measurements inside and outside. Independently, Nayak [15] developed those reported by Makinde and Animasaun [16] for finding the heat transfer characteristics in a 3-D water and ethylene glycol based Aluminum oxide nanofluid using the fourth order Runge-Kutta scheme.

In addition to the techniques discussed above, it is to be noted that Takhar et al. [17], Rao et al. [18], Singh and Mathew [19], Rudraswamy et al. [20] and Kar [21] obtained accurate results for the effective 3-D flow patterns. Motivated by our experience, this work is aimed to answer the crucial question of how an additional convergence can be applied to the homotopic based approach for solving the 3-D Casson fluid-driven flow past an exponentially stretching sheet. The rest of this work is organized as follows.

Section 2 provides a mathematical note on the Casson rheological model combined with governing differential equations. The solution methodology and its additional convergence are discussed in Sect. 3. Section 4 is exclusively devoted to the results and discussion. The main conclusions are presented in Sect. 5.

II. MATHEMATICAL FORMULATION

The constitutive equation for viscous stress tensor $\boldsymbol{\tau}$ in the Casson rheological model can be expressed alternatively in the form [22]:

$$\dot{\gamma} = \frac{1}{\mu_{\mathrm{C}}}\left(\sqrt{\boldsymbol{\tau}} - \sqrt{\tau_{\mathrm{C}}}\right)^2 \qquad (1)$$

where$\dot{\gamma}$ is the shear rate, μ_c is the Casson dynamic viscosity coefficient and τ_c is the Casson yield stress.

Based on the conservation of mass and linear momentum hypotheses, a 3-D fluid-driven flow through a porous medium is attained by the equations:

$$u_{,x} + v_{,y} + w_{,z} = 0 \qquad (2a)$$

$$uu_{,x} + vu_{,y} + wu_{,z} = \upsilon\left(1 + \frac{1}{\alpha_1}\right)u_{,zz} - \left(\frac{\sigma\mathcal{B}^2\sin^2\xi}{\rho} + \frac{\upsilon}{\alpha_2}\right)u, \quad (2b)$$

$$uv_{,x} + vv_{,y} + wv_{,z} = \upsilon\left(1 + \frac{1}{\alpha_1}\right)v_{,zz} - \left(\frac{\sigma\mathcal{B}^2\cos^2\xi}{\rho} + \frac{\upsilon}{\alpha_2}\right)v, \quad (2c)$$

with the boundary conditions,

$$\begin{aligned} &u = U_0 = U_1 e^{\frac{x+y}{L}}, v = V_0 = V_1 e^{\frac{x+y}{L}}, w = 0, \quad \text{at} \quad z = 0, \\ &u \to 0, v \to 0, \qquad\qquad \text{as } z \to \infty, \end{aligned} \quad (3)$$

where υ is the kinematic viscosity coefficient, α_1 is the Casson fluid parameter, σ is the electrical conductivity, $\mathcal{B}$ is the magnetic field strength, ξ is the inclination angle of magnetic field, ρ is the density, α_2 is the permeability of porous medium, U_0, U_1, V_0 and V_1 are the constant velocities and L is the characteristic length.

Upon introducing the quantities $\eta = \sqrt{\frac{U_1}{2\upsilon L}}e^{\frac{x+y}{2L}}z$, $u = U_1 e^{\frac{x+y}{L}}\varphi_{,\eta}$, $v = U_1 e^{\frac{x+y}{L}}\bar{\varphi}_{,\eta}$ and $w = -\sqrt{\frac{\upsilon U_1}{2L}}e^{\frac{x+y}{2L}}(\varphi + \bar{\varphi})$, the governing differential equations and associated boundary conditions become:

$$\left(1 + \frac{1}{\alpha_1}\right)\varphi_{,\eta\eta\eta} + (\varphi + \bar{\varphi})\varphi_{,\eta\eta} - \varphi_{,\eta}^2 - \left(\alpha_3^2\sin^2\xi + \alpha_4\right)\varphi_{,\eta} = 0, \quad (4a)$$

$$\left(1 + \frac{1}{\alpha_1}\right)\bar{\varphi}_{,\eta\eta\eta} + (\varphi + \bar{\varphi})\bar{\varphi}_{,\eta\eta} - \bar{\varphi}_{,\eta}^2 - \left(\alpha_3^2\cos^2\xi + \alpha_4\right)\bar{\varphi}_{,\eta} = 0, \quad (4b)$$

$$\begin{aligned} &\varphi = 0, \varphi_{,\eta} = 1, \bar{\varphi} = 0, \bar{\varphi}_{,\eta} = \alpha_5, \quad \text{at} \quad \eta = 0, \\ &\varphi_{,\eta} \to 0, \bar{\varphi}_{,\eta} \to 0, \qquad\qquad \text{as } \eta \to \infty, \end{aligned} \quad (5)$$

where $\alpha_3 = \sqrt{\frac{2\sigma\mathcal{B}^2 L}{\rho U_1}}$ is the magnetic field parameter, $\alpha_4 = \frac{\upsilon}{\alpha_2 U_1}$ is the porosity parameter and α_5 is the velocity ratio parameter.

Here, the local skin frictions can be defined as:

$$C_{\varphi x} = \frac{2\tau_{0x}}{\rho U_0^2}, C_{\bar{\varphi} y} = \frac{2\tau_{0y}}{\rho V_0^2}, \quad (6)$$

where,

$$\tau_{0x} = \mu_{\mathrm{C}}\left(1 + \frac{1}{\alpha_1}\right)u_{,z}|z = 0, \tau_{0y} = \mu_{\mathrm{C}}\left(1 + \frac{1}{\alpha_1}\right)v_{,z}|z = 0. \quad (7)$$

By substituting Eq. (7) into Eq. (6) and then rearrangement, one would get:

$$\sqrt{Re_x}C_{\varphi x} = \left(1 + \frac{1}{\alpha_1}\right)\varphi_{,\eta\eta}(0), \sqrt{Re_y}C_{\bar{\varphi} y} = \left(1 + \frac{1}{\alpha_1}\right)\left(\frac{V_1}{U_1}\right)\bar{\varphi}_{,\eta\eta}(0), \quad (8)$$

where $Re_x = \frac{U_0 L}{\upsilon}$ and $Re_y = \frac{V_0 L}{\upsilon}$ are the local Reynolds numbers along the x- and y-axes, respectively.

III. SOLUTION METHODOLOGY

Choosing an admissible interval of auxiliary parameter for analyzing nonlinear algebraic equations gives a uniformly convergent series expansion. According to the basic concept of *homotopy* in topology, a system of nonlinear boundary value problems (NBVPs) should be discretized to an infinite number of sub-NBVPs consisting of higher order derivatives expanded in some typical series expansions such as Taylor, Maclaurin, Laurent etc. [23, 24]. It is worth mentioning that the convergence of this scheme may be accelerated by means of minimizing the square residual error especially for those with the large intervals. Because, this minimization, which has seriously been proposed by KhoshrouyeGhiasi and Saleh [25-32], reduces the central processing unit (CPU) time (i.e., T_{CPU}) without the loss of accuracy. Hence, in view of the high nonlinearity involved in Eq. (4), a homotopy based approach will be developed here. To this end, the homotopy functions $\mathcal{H}_\varphi$ and $\mathcal{H}_{\bar{\varphi}}$ are constructed as [23]:

$$\mathcal{H}_\varphi[\varphi(\eta;q), \bar{\varphi}(\eta;q); q] = (1-q)\mathcal{L}_\varphi[\varphi(\eta;q) - \varphi_0(\eta)] + q\hbar_\varphi\mathcal{N}_\varphi[\varphi(\eta;q), \bar{\varphi}(\eta;q)], \quad (9a)$$

$$\mathcal{H}_{\bar{\varphi}}[\varphi(\eta;q), \bar{\varphi}(\eta;q); q] = (1-q)\mathcal{L}_{\bar{\varphi}}[\bar{\varphi}(\eta;q) - \bar{\varphi}_0(\eta)] + q\hbar_{\bar{\varphi}}\mathcal{N}_{\bar{\varphi}}[\varphi(\eta;q), \bar{\varphi}(\eta;q)], \quad (9b)$$

where $q \in [0,1]$ is an embedding parameter, $\mathcal{L}_\varphi$ and $\mathcal{L}_{\bar{\varphi}}$ are the auxiliary linear operators, φ_0 and $\bar{\varphi}_0$ are the initial guesses, $\hbar_\varphi$ and $\hbar_{\bar{\varphi}}$ are the nonzero auxiliary parameters, and $\mathcal{N}_\varphi$ and $\mathcal{N}_{\bar{\varphi}}$ are the nonlinear operators. Since $\varphi(\eta;q)$ and $\bar{\varphi}(\eta;q)$ increase from the initial guesses to the exact solutions as q is increased from 0 to 1, the bounds are obtained by setting Eq. (9) equal to zero. Also expanding $\varphi(\eta;q)$ and $\bar{\varphi}(\eta;q)$ in a Taylor's series with respect to q gives:

$$\varphi(\eta;q) = \varphi_0(\eta;0) + \sum_{j=1}^{\infty}\frac{1}{j!}\varphi_{,q}^{(j)}(\eta;q)\,|q = 0 = \varphi_0(\eta) + \sum_{j=1}^{\infty}\varphi_j(\eta)q^j, \quad (10a)$$

$$\bar{\varphi}(\eta;q) = \bar{\varphi}_0(\eta;0) + \sum_{j=1}^{\infty}\frac{1}{j!}\bar{\varphi}_{,q}^{(j)}(\eta;q)\,|q = 0 = \bar{\varphi}_0(\eta) + \sum_{j=1}^{\infty}\bar{\varphi}_j(\eta)q^j, \quad (10b)$$

where φ_j and $\bar{\varphi}_j$ are the jth-order approximate derivatives.

It is to be noted that by setting Eq. (9) and q equal to zero, the so-called zeroth-order deformation equations can be rewritten as [23]:

$$\mathcal{L}_\varphi[\varphi(\eta;0) - \varphi_0(\eta)] = 0, \mathcal{L}_{\bar{\varphi}}[\bar{\varphi}(\eta;0) - \bar{\varphi}_0(\eta)] = 0. \quad (11)$$

By differentiating $\mathcal{H}_{\varphi}[\varphi(\eta;q),\bar{\varphi}(\eta;q);q]=0$ and $\mathcal{H}_{\bar{\varphi}}[\varphi(\eta;q),\bar{\varphi}(\eta;q);q]=0$, j times with respect to q, setting $q=0$ and then dividing them by $j!$, the$j$th-order deformation equations are obtained as:

$$\mathcal{L}_{\varphi}\left[\varphi_j(\eta)-\chi_j\varphi_{j-1}(\eta)\right]+\frac{1}{(j-1)!}\hbar_{\varphi}\mathcal{N}_{\varphi,q}^{(j-1)}[\varphi(\eta;q),\bar{\varphi}(\eta;q)]|q=0=0, \quad (12a)$$

$$\mathcal{L}_{\bar{\varphi}}\left[\bar{\varphi}_j(\eta)-\chi_j\bar{\varphi}_{j-1}(\eta)\right]+\frac{1}{(j-1)!}\hbar_{\bar{\varphi}}\mathcal{N}_{\bar{\varphi},q}^{(j-1)}[\varphi(\eta;q),\bar{\varphi}(\eta;q)]|q=0=0, \quad (12b)$$

where,

$$\chi_j=\begin{cases}0, & j\le 1,\\ 1, & j>1.\end{cases} \quad (13)$$

It is desirable to apply the same procedure on the governing Eq. (4) and its associated boundary conditions given in Eq. (5). To this end, the initial approximations and auxiliary linear operators are selected as:

$$\varphi_0(\eta)=1-e^{-\eta},\bar{\varphi}_0(\eta)=\alpha_5(1-e^{-\eta}), \quad (14)$$

$$\mathcal{L}_{\varphi}=\varphi_{,\eta\eta\eta}(\eta)-\varphi_{,\eta}(\eta),\mathcal{L}_{\bar{\varphi}}=\bar{\varphi}_{,\eta\eta\eta}(\eta)-\bar{\varphi}_{,\eta}(\eta), \quad (15)$$

with the properties,

$$\mathcal{L}_{\varphi}[\kappa_1+\kappa_2e^{\eta}+\kappa_3e^{-\eta}]=0,\mathcal{L}_{\bar{\varphi}}[\kappa_4+\kappa_5e^{\eta}+\kappa_6e^{-\eta}]=0, \quad (16)$$

whereκ_1-κ_6 are the integration constants. The functions $\varphi(\eta;q)$ and $\bar{\varphi}(\eta;q)$ can be expanded in a Taylor's series in the form:

$$\varphi(\eta;q)=\varphi_0(\eta)+q\varphi_1(\eta)+q^2\varphi_2(\eta)+\cdots,\bar{\varphi}(\eta;q)=\bar{\varphi}_0(\eta)+q\bar{\varphi}_1(\eta)+q^2\bar{\varphi}_2(\eta)+\cdots. \quad (17)$$

The nonlinear operators involved in Eq. (9) are given by:

$$\mathcal{N}_{\varphi}[\varphi(\eta;q),\bar{\varphi}(\eta;q)]=\left(1+\frac{1}{\alpha_1}\right)\varphi_{,\eta\eta\eta}(\eta;q)+\left(\varphi(\eta;q)+\bar{\varphi}(\eta;q)\right)\varphi_{,\eta\eta}(\eta;q)-\varphi_{,\eta}^2(\eta;q)-\left(\alpha_3^2\sin^2\xi+\alpha_4\right)\varphi_{,\eta}(\eta;q)=0, \quad (18a)$$

$$\mathcal{N}_{\bar{\varphi}}[\varphi(\eta;q),\bar{\varphi}(\eta;q)]=\left(1+\frac{1}{\alpha_1}\right)\varphi_{,\eta\eta\eta}(\eta;q)+\left(\varphi(\eta;q)+\bar{\varphi}(\eta;q)\right)\varphi_{,\eta\eta}(\eta;q)-\varphi_{,\eta}^2(\eta;q)-\left(\alpha_3^2\cos^2\xi+\alpha_4\right)\varphi_{,\eta}(\eta;q)=0. \quad (18b)$$

The zeroth-order deformation equations in this case are assumed to be:

$$\varphi_{,\eta\eta\eta}(\eta)-\varphi_{0,\eta}(\eta)=0,\bar{\varphi}_{,\eta\eta\eta}(\eta)-\bar{\varphi}_{0,\eta}(\eta)=0, \quad (19)$$

with the boundary conditions,

$$\varphi(\eta;q)=0,\varphi_{,\eta}(\eta;q)=1,\bar{\varphi}(\eta;q)=0,\bar{\varphi}_{,\eta}(\eta;q)=\alpha_5,\quad \text{at}\quad \eta=0,\qquad \varphi_{,\eta}(\eta;q)\to 0,\bar{\varphi}_{,\eta}(\eta;q)\to 0,\quad \text{as}\ \eta\to\infty. \quad (20)$$

Hence, the jth-order deformation equations are constructed as:

$$\varphi_{j,\eta\eta\eta}(\eta)-\varphi_{j,\eta}(\eta)=\chi_j\left(\varphi_{j-1,\eta\eta\eta}(\eta)-\varphi_{j-1,\eta}(\eta)\right)-\frac{1}{(j-1)!}\hbar_{\varphi}\mathcal{N}_{\varphi,q}^{(j-1)}[\varphi(\eta;q),\bar{\varphi}(\eta;q)]|q=0=0, \quad (21a)$$

$$\bar{\varphi}_{j,\eta\eta\eta}(\eta)-\bar{\varphi}_{j,\eta}(\eta)=\chi_j\left(\bar{\varphi}_{j-1,\eta\eta\eta}(\eta)-\bar{\varphi}_{j-1,\eta}(\eta)\right)-\frac{1}{(j-1)!}\hbar_{\bar{\varphi}}\mathcal{N}_{\bar{\varphi},q}^{(j-1)}[\varphi(\eta;q),\bar{\varphi}(\eta;q)]|q=0=0, \quad (21b)$$

which goes to zero boundary conditions. After finding the integration constants κ_1-κ_5, the jth-order approximate solutions of Eq. (21) take the form:

$$\varphi_j(\eta)=\varphi_j^{\blacksquare}(\eta)-\varphi_j^{\blacksquare}(0)+1-\varphi_{j,\eta}^{\blacksquare}(0)(1-e^{-\eta}), \quad (22a)$$

$$\bar{\varphi}_j(\eta)=\bar{\varphi}_j^{\blacksquare}(\eta)-\bar{\varphi}_j^{\blacksquare}(0)+\alpha_5-\bar{\varphi}_{j,\eta}^{\blacksquare}(0)(\alpha_5-e^{-\eta}), \quad (22b)$$

where$\varphi_j^{\blacksquare}(\eta)$ and $\bar{\varphi}_j^{\blacksquare}(\eta)$ are the particular solutions. Hence, the pth-order approximate solutions are calculated as:

$$\varphi_p(\eta)=\sum_{j=0}^{p}\varphi_j(\eta),\bar{\varphi}_p(\eta)=\sum_{j=0}^{p}\bar{\varphi}_j(\eta). \quad (23)$$

Here, the square residual errors are expressed as [33]:

$$\Delta_p^{\varphi}=\frac{1}{i+1}\sum_{n=0}^{i}\left(\mathcal{N}_{\varphi}\left[\sum_{m=0}^{p}\varphi(\eta),\sum_{m=0}^{p}\bar{\varphi}(\eta)\right]|\eta=n\delta\eta\right)^2, \quad (24a)$$

$$\Delta_p^{\bar{\varphi}}=\frac{1}{i+1}\sum_{n=0}^{i}\left(\mathcal{N}_{\bar{\varphi}}\left[\sum_{m=0}^{p}\varphi(\eta),\sum_{m=0}^{p}\bar{\varphi}(\eta)\right]|\eta=n\delta\eta\right)^2, \quad (24b)$$

where,

$$\Delta_{p,\hbar_{\varphi}}^{\varphi}\left(\hbar_{\varphi}\right)=0,\Delta_{p,\hbar_{\bar{\varphi}}}^{\bar{\varphi}}\left(\hbar_{\bar{\varphi}}\right)=0. \quad (25)$$

IV. RESULTS AND DISCUSSION

To validate the accuracy and reliability of the above homotopy based approach, the geometric and physical properties involved in Eqs. (4) and (5), unless stated otherwise, are represented in Table 1. It is to be mentioned here that the physical properties given in Table 1 have been selected in such a way that they match with the case studied by Butt et al. [34], and the only discrepancy could be due to the negligible unsteadiness. Furthermore, the auxiliary parameters reported by Butt et al. [34], that did not take into account any additional

convergence of the homotopy based approach, are assumed to be $\hbar_{\varphi} = \hbar_{\bar{\varphi}} = -0.3$. In view of the results shown in Tables 2 and 3, it is evident that the 9th-order homotopy based approach is so accurate compared to that reported by Yousif et al. [35]; because the relative error in these two cases does not exceed 0.097% and 0.209%.

Tables 2 and 3 respectively provide the variation of local skin friction along the x- and y-axes versus values of the porosity parameter. According to these tables, the local skin frictions in both cases enhance when the porosity parameter is increased. Hence, a high accuracy approximation can be expected if the 9th-order homotopy based approach is employed.

Table 1. Geometric and physical properties.

α_1	α_3	ξ	α_4	α_5
0.3	1	45°	0.5	0.5

Table 2. Verification of the local skin friction along the x-axis with physical properties $\alpha_1 = 1$ and $\alpha_3 = 0$.

α_4	Present ($\hbar_{\varphi} = -0.3$)			DTM-Padé [35]
	$p = 5$	$p = 7$	$p = 9$	
0	1.5411	1.5429	1.5451	1.5472
0.5	1.8319	1.8335	1.8352	1.8363
1	2.0827	2.0844	2.0865	2.0885

Table 3. Verification of the local skin friction along the y-axis with physical properties $\alpha_1 = 1$ and $\alpha_3 = 0$.

α_4	Present ($\hbar_{\bar{\varphi}} = -0.3$)			DTM-Padé [35]
	$p = 5$	$p = 7$	$p = 9$	
0	0.6540	0.6552	0.6569	0.6589
0.5	0.8176	0.8195	0.8217	0.8230
1	0.9549	0.9573	0.9598	0.9614

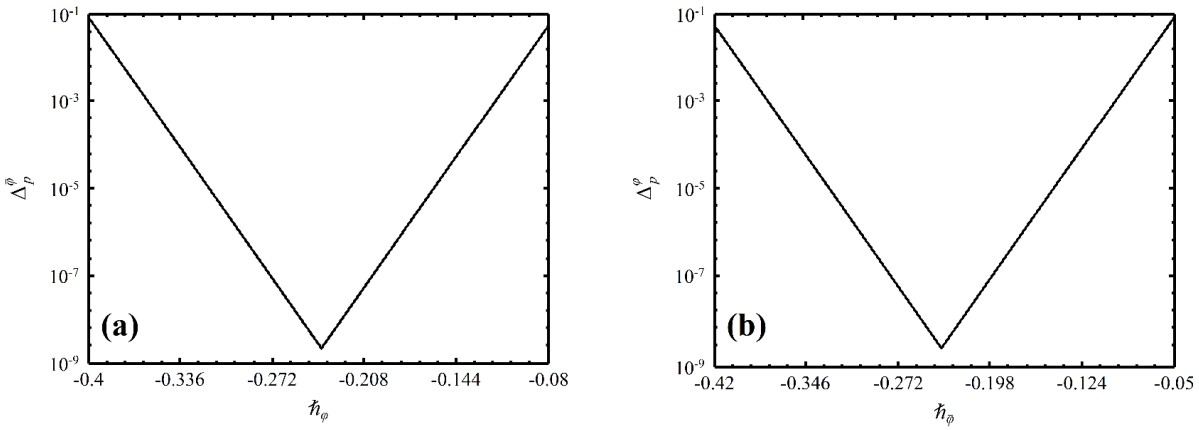

Fig. 1. Selection of **a**$\hbar_{\varphi}$ and **b**$\hbar_{\bar{\varphi}}$.

The variation of square residual errors versus values of the auxiliary parameters with properties given in Table 1 is depicted in Fig. 1 for the case $p = 9$. As it is seen from this figure, the square residual errors will be minimized while the auxiliary parameters are selected as $\hbar_{\varphi} = -0.243$ and $\hbar_{\bar{\varphi}} = -0.243$. To explain more, optimal values of the auxiliary parameters and associated CPU times as well as minimum values of the square residual errors are reported in Tables 4 and 5.

Based on the results presented in Tables 4 and 5, by increasing values of p the square residual errors clearly reduce which is only due to the additional convergence of this scheme. This fact can be desirable to achieve a series expansion with a faster rate of convergence.

In Tables 6 and 7, the accuracy of 9th-order homotopy based approach with and without using optimal values of the auxiliary parameters is compared with that reported by homotopy perturbation method (HPM) [36] and a closed-form solution [24]. According to these tables, it is observed that the 9th-order homotopy based approach combined with $\hbar_{\varphi} = -0.243$ and $\hbar_{\bar{\varphi}} = -0.243$ agrees remarkably well with those presented by Ariel [36, 37]. Hence, using the 9th-order homotopy based approach with $\hbar_{\varphi} = -0.243$ and $\hbar_{\bar{\varphi}} = -0.243$ is strongly suggested; only because it can provide more accurate results than those of $\hbar_{\varphi} = \hbar_{\bar{\varphi}} = -0.3$. Furthermore, Tables 6 and 7 show the effect of velocity ratio parameter on reducing the axial and transverse velocities, respectively.

It is to be mentioned here that a similar conclusion regarding micro-convection model of nanofluids past an exponentially stretching sheet has also been presented by Nayak et al. [38].

In view of the available results depicted in Table 8, one can conclude that the velocity distribution essentially converges for $\hbar_{\varphi}$ = -0.243 and $\hbar_{\bar{\varphi}}$ = -0.243. With this important observation, the combined effects of Casson fluid parameter and inclined magnetic field on the variation of local skin friction is given in Table 9. From this table, it is seen that the local skin friction is an enhancing function of $\alpha_3$and ξ,while it is a diminishing function of α_1.

Table 4. Convergence of series expansion along the x-axis with the properties given in Table 1, when the CPU time is subjected to two digits.

η	$p = 5$			$p = 7$			$p = 9$		
	$\hbar_{\varphi,\text{opt}}$	Δ_p^{φ}	T_{CPU} (s)	$\hbar_{\varphi,\text{opt}}$	Δ_p^{φ}	T_{CPU} (s)	$\hbar_{\varphi,\text{opt}}$	Δ_p^{φ}	T_{CPU} (s)
0	-0.282	8.24×10^{-7}	5.11	-0.257	4.01×10^{-7}	10.19	-0.243	8.55×10^{-8}	25.36
0.2	-0.282	8.76×10^{-7}	5.11	-0.257	4.50×10^{-7}	10.19	-0.243	9.02×10^{-8}	25.36
0.4	-0.282	9.29×10^{-7}	5.11	-0.257	4.96×10^{-7}	10.19	-0.243	9.61×10^{-8}	25.36
0.6	-0.282	9.83×10^{-7}	5.11	-0.257	5.48×10^{-7}	10.19	-0.243	1.14×10^{-7}	25.36
0.8	-0.282	1.26×10^{-6}	5.11	-0.257	6.09×10^{-7}	10.19	-0.243	1.70×10^{-7}	25.36
1	-0.282	1.89×10^{-6}	5.11	-0.257	6.73×10^{-7}	10.19	-0.243	2.37×10^{-7}	25.36

Table 5. Convergence of series expansion along the y-axis with the properties given in Table 1, when the CPU time is subjected to two digits.

η	$p = 5$			$p = 7$			$p = 9$		
	$\hbar_{\bar{\varphi},\text{opt}}$	$\Delta_p^{\bar{\varphi}}$	T_{CPU} (s)	$\hbar_{\bar{\varphi},\text{opt}}$	$\Delta_p^{\bar{\varphi}}$	T_{CPU} (s)	$\hbar_{\bar{\varphi},\text{opt}}$	$\Delta_p^{\bar{\varphi}}$	T_{CPU} (s)
0	-0.272	9.52×10^{-7}	6.66	-0.240	3.71×10^{-7}	11.70	-0.236	7.14×10^{-8}	30.90
0.2	-0.272	1.23×10^{-6}	6.66	-0.240	4.02×10^{-7}	11.70	-0.236	8.88×10^{-8}	30.90
0.4	-0.272	1.79×10^{-6}	6.66	-0.240	4.56×10^{-7}	11.70	-0.236	9.30×10^{-8}	30.90
0.6	-0.272	2.45×10^{-6}	6.66	-0.240	5.22×10^{-7}	11.70	-0.236	9.81×10^{-8}	30.90
0.8	-0.272	3.29×10^{-6}	6.66	-0.240	5.76×10^{-7}	11.70	-0.236	1.19×10^{-7}	30.90
1	-0.272	3.91×10^{-6}	6.66	-0.240	6.31×10^{-7}	11.70	-0.236	1.61×10^{-7}	30.90

Table 6. Effect of $\hbar_{\bar{\varphi},\text{opt}}$ on the local skin fiction along the x-axis. The values in parentheses are those obtained through $\hbar_{\bar{\varphi}}$ = -0.3.

α_5	Present			HPM [36]	Exact [37]
	$p = 5$	$p = 7$	$p = 9$		
0	1 (1)	1 (1)	1 (1)	1	1
0.5	1.092705 (1.092622)	1.092799 (1.092746)	1.092886 (1.092855)	1.088662	1.093095
1	1.172488 (1.172418)	1.172583 (1.172522)	1.172666 (1.172632)	1.178511	1.173721

Table 7. Effect of $\hbar_{\bar{\varphi},\text{opt}}$ on the local skin fiction along the y-axis. The values in parentheses are those obtained through $\hbar_{\bar{\varphi}}$ = -0.3.

α_5	Present			HPM [36]	Exact [37]
	$p = 5$	$p = 7$	$p = 9$		
0	0 (0)	0 (0)	0 (0)	0	0
0.5	0.463550 (0.463521)	0.463591 (0.463571)	0.464014 (0.464002)	0.476290	0.465205
1	1.172527 (1.172480)	1.172641 (1.172599)	1.172688 (1.172661)	1.178511	1.173721

Table 8. Velocity distribution with geometric and physical properties given in Table 1.

η	$\varphi_{,\eta}(\eta)$		$\bar{\varphi}_{,\eta}(\eta)$	
	$\hbar_{\varphi}$ = -0.3	$\hbar_{\varphi,\text{opt}}$ = -0.243	$\hbar_{\bar{\varphi}}$ = -0.3	$\hbar_{\bar{\varphi},\text{opt}}$ = -0.236
0	1	1	0.5	0.5
0.1	0.9436	0.8621	0.4902	0.4329
0.2	0.8615	0.7995	0.4580	0.3720
0.3	0.7720	0.6951	0.3920	0.3219
0.4	0.6793	0.6340	0.3432	0.2524
0.5	0.6204	0.5517	0.3012	0.1976
0.6	0.5380	0.4614	0.2470	0.1249
0.7	0.4601	0.3522	0.2135	0.0942
0.8	0.3917	0.2396	0.1573	0.0231

0.9	0.3318	0.1570	0.1046	0.0057
1	0.2314	0.0831	0.0534	0
2	0.1170	0.0096	0.0072	0
3	0.0812	0	0	0
4	0.0246	0	0	0
5	0.0019	0	0	0
6	0	0	0	0

V. CONCLUSION

This work was devoted to optimizing the homotopy based approach for 3-D Casson fluid-driven flow under external magnetic field. A comparison of this scheme with other cases proved that the 9th-order homotopy based approach results in fast and accurate calculations. Furthermore, it was shown that this scheme can be regarded as a useful tool for solving strongly nonlinear differential equations at some time in the future.

REFERENCES

[1]. H. Schlichting, Boundary layer theory (8th edn.). Berlin: Springer; 2000.
[2]. J. Tu, H. Yeoh, C. Liu, Computational fluid dynamics: A practical approach. New York: Butterworth-Heinemann; 2007.
[3]. N. Sandeep, O.K. Koriko, I.L. Animasaun, Modified kinematic viscosity model for 3D-Casson fluid flow within boundary layer formed on a surface at absolute zero, J. Mol. Liq. 221 (2016) 1197-1206.
[4]. J.C. Williams, T.H. Rhyne, Boundary layer development on a wedge impulsively set into motion, SIAM J. Appl. Math. 38 (1980) 215-224.
[5]. S.A. Shehzad, T. Hayat, A. Alsaedi, M.A. Meraj, Cattaneo-Christov heat and mass flux model for 3D hydrodynamic flow of chemically reactive Maxwell liquid, Appl. Math. Mech.-Eng. Ed. 38(10) (2017) 1347-1356.
[6]. M.K. Nayak, MHD 3D flow and heat transfer analysis of nanofluid by shrinking surface inspired by thermal radiation and viscous dissipation, Int. J. Mech. Sci. 124-125 (2017) 185-193.
[7]. F.U. Rehman, S. Nadeem, H.U. Rehman, R. UlHaq, Thermophysical analysis for three-dimensional MHD stagnation-point flow of nano-material influenced by an exponential stretching surface, Results Phys. 8 (2018) 316-323.
[8]. T. Hayat, I. Ullah, T. Muhammad, A. Alsaedi, Radiative three-dimensional flow with Soret and Dufour effects, Int. J. Mech. Sci. 133 (2017) 829-837.
[9]. T. Hayat, I. Ullah, T. Muhammad, A. Alsaedi, Magnetohydrodynamic (MHD) three-dimensional flow of second grade nanofluid by a convectively heated exponentially stretching surface, J. Mol. Liq. 220 (2016) 1004-1012.
[10]. S.A. Shehzad, T. Hayat, A. Alsaedi, MHD three dimensional flow of viscoelastic fluid with thermal radiation and variable thermal conductivity, J. Cent. South Univ. 21(10) (2014) 3911-3917.
[11]. S.A. Shehzad, T. Hayat, A. Alsaedi, MHD three-dimensional flow of viscoelastic fluid with convective surface boundary condition, J. Eng. Thermophys. 27(1) (2018) 106-118.
[12]. A. Alsaedi, T. Hayat, T. Muhammad, S.A. Shehzad, MHD three-dimensional flow of viscoelastic fluid over an exponentially stretching surface with variable thermal conductivity, Comput. Math. Math. Phys. 56(9) (2016) 1665-1678.
[13]. M.B. Ashraf, T. Hayat, S. Shehzad, B. Ahmed, Thermophoresis and MHD mixed convection three-dimensional flow of viscoelastic fluid with Soret and Dufour effects, Neural Comput. Appl. 31(1) (2019) 249-261.
[14]. D. Lu, M. Ramzan, M. Bilal, J.D. Chung, U. Farooq, S. Tahir, On three-dimensional MHD Oldroyd-B fluid with nonlinear thermal radiation and homogeneous-heterogeneous reaction, J. Braz. Soc. Mech. Sci. Eng. 40(8) (2018) 1-11.
[15]. M.K. Nayak, S. Shaw, V.S. Pandey, A.J. Chamkha, Combined effects of slip and convective boundary condition on MHD 3D stretched flow of nanofluid through porous media inspired by non-linear thermal radiation, Ind. J. Phys. 92(8) (2018) 1017-1028.
[16]. O.D. Makinde, I.L. Animasaun, Bioconvection in MHD nanofluid flow with nonlinear thermal radiation and quartic autocatalysis chemical reaction past an upper surface of a paraboloid of revolution, Int. J. Therm. Sci. 109 (2016) 159-171.
[17]. H.S. Takhar, A.J. Chamkha, G. Nath, Unsteady three-dimensional MHD-boundary-layer flow due to the impulsive motion of a stretching surface, Acta Mech. 146(1-2) (2001) 59-71.
[18]. M.V. S. Rao, K. Gangadhar, P.L.N. Varma, A spectral relaxation method for three-dimensional MHD flow of nanofluid flow over an exponentially stretching sheet due to convective heating: an application to solar energy, Indian J. Phys. 92(12) (2018) 1577-1588.
[19]. K.D. Singh, A. Mathew, Heat and mass transfer on unsteady three-dimensional convective MHD flow past a porous plate moving in a parallel free stream, Indian J. Phys. 83(10) (2009) 1439-1455.
[20]. N.G. Rudraswamy, S.A. Shehzad, K. Ganesh Kumar, B.J. Gireesha, Numerical analysis of MHD three-dimensional Carreaunanoliquid flow over bidirectionally moving surface, J. Braz. Soc. Mech. Sci. Eng. 39(12) (2017) 5037-5047.
[21]. M. Kar, G.C. Dash, S.N. Sahoo, P.K. Rath, Three-dimensional free convection MHD flow in a vertical channel through a porous medium with heat source and chemical reaction, J. Eng. Thermophys. 22(3) (2013) 203-215.
[22]. N. Casson, Rheology of disperse systems. New York: C.C. Mill; 1959.
[23]. S.J. Liao, Beyond perturbation: Introduction to the homotopy analysis method. Boca Raton: Chapman & Hall/CRC Press; 2003.
[24]. S.J. Liao, Notes on the homotopy analysis method: Some definitions and theorems, Commun. Nonlinear Sci. Numer. Simulat. 14(4) (2009) 983-997.
[25]. E. KhoshrouyeGhiasi, R. Saleh, Unsteady shrinking embedded horizontal sheet subjected to inclined Lorentz force and Joule heating, an analytical solution, Results Phys. 11 (2018) 65-71.
[26]. E. KhoshrouyeGhiasi, R. Saleh, Homotopy analysis method for the Sakiadis flow of a thixotropic fluid, Eur. Phys. J. Plus 134(1) (2019) 1-9.
[27]. E. KhoshrouyeGhiasi, R. Saleh, Constructing analytic solutions on the Tricomi equation, Open Phys. 16(1) (2018) 143-148.
[28]. E. KhoshrouyeGhiasi, R. Saleh, Nonlinear stability and thermomechanical analysis of hydromagnetic Falkner-SkanCasson conjugate fluid flow over an angular-geometric surface based on Buongiorno's model using homotopy analysis method and its extension, Pramana 92(1) (2019) 1-12.
[29]. E. KhoshrouyeGhiasi, R. Saleh, A convergence criterion for tangent hyperbolic fluid along a stretching wall subjected to inclined electromagnetic field, SeMA J. 76(3) (2019) 521-531.
[30]. E. KhoshrouyeGhiasi, R. Saleh, 2D flow of Casson fluid with non-uniform heat source/sink and Joule heating, Front. Heat Mass Trans. 12 (2019) 1-7.

[31]. E. KhoshrouyeGhiasi, R. Saleh, Thermophysical investigation of unsteady Casson-Carreau fluid, INAE Lett. 4(4) (2019) 227-239.
[32]. E. KhoshrouyeGhiasi, R. Saleh, Analytical and numerical solutions to the 2D Sakiadis flow of Casson fluid with cross diffusion, inclined magnetic force, viscous dissipation and thermal radiation based on Buongiorno's mathematical model, CFD Lett. 11(1) (2019) 40-54.
[33]. S.J. Liao, An optimal homotopy-analysis approach for strongly nonlinear differential equations, Commun. Nonlinear Sci. Numer. Simulat. 15(8) (2010) 2003-2016.
[34]. A.S. Butt, M.N. Tufail, A. Ali, Three-dimensional flow of a magnetohydrodynamicCasson fluid over an unsteady stretching sheet embedded into a porous medium, J. Appl. Mech. Tech. Phys. 57(2) (2016) 283-292.
[35]. M.A. Yousif, M. Hatami, H.F. Esmael, Heat transfer analysis of MHD three dimensional Casson fluid flow over a porous stretching sheet by DTM-Padé, Int. J. Appl. Comput. Math. 3(1) (2017)813-828.
[36]. P.D. Ariel, The three-dimensional flow past a stretching sheet and the homotopy perturbation method, Comput. Math. Appl. 54(7-8) (2007) 920-925.
[37]. P.D. Ariel, Generalized three-dimensional flow due to a stretching sheet, ZAMM. Z. Angew. Math. Mech. 83(12) (2003) 844-852.
[38]. M.K. Nayak, S. Shaw, A.J. Chamkha, 3D MHD free convective stretched flow of a radiativenanofluid inspired by variable magnetic field, Arab. J. Sci. Eng. 44(2) (2019) 1269-1282.

EmranKhoshrouye Ghiasi. "3-D exponentially Casson fluid-driven flow under inclined magnetic field: A convergent series expansion." *International Journal of Engineering Science Invention (IJESI)*, Vol. 09(08), 2020, PP 07-10. Journal DOI- 10.35629/6734